Research Article Adv. Mater. Lett. 2015, **6**(10), 867-873 Advanced Materials *Letters*

www.amlett.com, www.vbripress.com/aml, DOI: 10.5185/amlett.2015.5858 Published online by the VBRI Press in 2015

Aqueous phase photodegradation of rhodamine B and p-nitrophenol desctruction using titania based nanocomposites

Suranjan Sikdar[1], Sayantan Pathak[1], Tanmay K Ghorai[1,2*]

[1]*Department of Chemistry, University of Gour Banga, Malda 732103, West Bengal, India*
[2]*Department of Chemistry, West Bengal State University, Barasat, Kolkata 700126, West Bengal, India*

[*]Corresponding author. Tel: (+91) 3512 223664; E-mail: tghorai@ugb.ac.in; tanmayghorai66@gmail.com

Received: 17 February 2015, Revised: 19 August 2015 and Accepted: 29 August 2015

ABSTRACT

Heterogeneous photocatalysts offer great potential for converting photon energy into chemical energy for decomposition and destruction of organic contaminants from organic molecules i.e. Rhodamine B (RhB) and p-nitophenol (p-NP) under UV light. The titania based novel $M_xNb_xTi_{1-2x}O_{2-x/2}$ (M = Cr, Fe; x = 0.01-0.2) was prepared by tetra and tri-podal amine type binder with iron or chromium support using sol–gel method followed by calcination at 150 ^oC in an auto generated pressure. The photodegradation performance of the optimized catalyst was compared with synthesized nano-compositions, P-25 titania with RhB and p-NP. The particle sizes, surface area, mesopore sizes of $Cr_xNb_xTi_{1-2x}O_{2-x/2}$ (x = 0.01) (CNT1) and $Fe_xNb_xTi_{1-}2xO_{2-x/2}$ (x = 0.01) (FNT1) are 12±1 and 10±2 nm, S_{BET}=162 and 145 m^2g^{-1}, 4.9 and 4-5 nm, respectively. The energy band gap of CNT1, FNT1 and NT was found to be 1.85, 2.06 and 2.1 eV, respectively. The importance of CNT1 powders is that it shows good photocatalytic activity for the degradation of Rhodamine B (RhB) within only 180 min and the importance of FNT1 powders is that it reduces the p-NP to p-aminophenol using a little bit of $NaBH_4$ (0.054 g) within 10 min as compared to pure anatase TiO_2 and other compositions of $M_xNb_xTi_{1-2x}O_{2-x/2}$ (M = Cr, Fe). Copyright © 2015 VBRI Press.

Keywords: Titanium dioxide; sol-gel synthesis; nano-composites; RhB; p-NP.

Introduction

The fact that the human health always gets threatened from phenol based compounds is well-known and the presence of phenol derivatives in a wide range of locations from industrial waste water to agricultural waste represents an important challenge for environmental protection. The role of benzene rings in all of the phenol moieties has a strong inhibitive function for biological degradation. Therefore it is very difficult to degrade them into small inorganic molecules by using traditional route [**1, 2**]. Typically phenols are used extensively in chemical industries for the production of different kind of pesticides, pharmaceutical and synthetic dyes [**3, 4**]. Nitrophenols can damage the central nervous system, liver, kidney and blood of animals and humans. Similarly, water contaminated dyes i.e. methyl orange, rhodamine B, thymolblue etc. are also threat to the environment [**5-7**] and accountable for skin cancer. Degradation of these toxic substances by photocatalysis in aqueous medium could be the basis of a waste treatment method [**8, 9**]. Therefore, photocatalysis is an important method for degradation of organic pollutants through efficiently conversion of solar energy into chemical energy [**10-12**].

In this context, mesoporous compounds have an important role in photochemical reactions for removal of such type of pollutants. Mesoporous titanium dioxide (TiO_2) based semiconductors have continued to be highly efficient in photocatalytic applications because of its high surface area and porous frameworks. In the past decade, there have been few reports about mesoporous transition-metal oxides [**13-16**]. Ismail *et al.* found that TiO_2 microspheres with porous structures have higher photocatalytic activity and they can be easily recovered for their re-use as catalysts [**13**]. Furthermore, photoactivity is highly dependent on surface area and crystallinity or crystal sizes, which are in turn influenced by the synthetic methods of titania synthesis [**14, 15**].

The most recent studies show that the addition of small quantities of Nb_2O_5 into TiO_2 lattice significantly increases the photocatalytic activity and surface acidity of TiO_2 [**16, 17**]. On the other hand, Cr(III) or Fe(III) doped photocrystalline titania/zinc oxide have also been widely studied in the field of photocatalysis [**18-24**]. The effect of simultaneous mixed oxides of Cr/Fe and Nb in TiO_2 mesoporous structure and its photocatalytic activity has not yet been reported. Moreover, the interesting observation was CNT1 has more photodegradation properties on RhB

and FNT1 has good reduction properties on p-NP in comparison with other compositions.

In this present work, we report the synthesis and characterization of mesoporous $M_xNb_xTi_{1-2x}O_{2-x/2}$ (M = Cr, Fe; x = 0.01) with a surface area of up to 162 m^2g^{-1} prepared from a titanium/niobium tartarate with N, N, N', N'-tetrakis(2-hydroxyethyl)ethylenediamine, triethanol amine, chromium and ferric nitrate precursor by sol-gel method. Here, the role of Cr(III) or Fe(III) in M-Nb-TiO_2 composite is to compensate the charge imbalance caused by the replacement of Ti(IV) with Nb(V) in TiO_2 crystals, which results improvement of charge separation among the photo-produced hole-electron pairs.

Experimental

Chemicals required

Titanium dioxide (analytical reagent), Nb_2O_5 (analytical reagent), $(NH_4)_2Cr_2O_7$ (analytical reagent), $Fe(NO_3)_3$ $6H_2O$ (analytical reagent), NaOH (analytical reagent), HF (40%), tartaric acid, and NH_4OH (25%), HF (40%), methanol, ethanol, N, N, N', N'-tetrakis(2-hydroxyethyl) ethylenediamine ($edteH_4$) (Sigma Aldrich) , triethanolamine (TEA), Rhodamine B and 4-nitrophenol (4-NP) were of analytical reagent grade and were procured from B.D.H., India.

Synthesis of $M_xNb_xTi_{1-2x}O_{2-x/2}$ (x = Cr, Fe) nano-composites

Nano-composites of $M_xNb_xTi_{1-2x}O_{2-x/2}$ (M = Cr, Fe; x = 0.01, 0.05, 0.1, 0.2) were prepared by sol-gel method. The total synthesis was carried out in two steps. In the first step, the stock solutions of chromium and ferric nitrate, titanium and niobium tartarate solutions were prepared. The solution of the titanium and niobium tartarate, which are not commercially available were prepared in the laboratory from its hydrated oxide (Nb_2O_5 nH_2O and TiO_2 nH_2O); the details of the preparation processes are discussed elsewhere [**6, 20, 25**]. In the second step, in Set-I, stoichiometric amounts of titanium and niobium tartarate, ammonium dichromate with complexing agent N, N, N', N'-tetrakis(2-hydroxyethyl) ethylenediamine ($edteH_4$) (molar ratio of metal ion: edteH4 = 1:2) and 20 mL of absolute ethanol solutions were taken in a beaker as per the predetermined chemical compositions (example shown for x = 0.01) with constant stirring for 30 min at room temperature. In Set-II ammonium dichromate and $edteH_4$ is replaced by ferric nitrate and triethanolamine (3 mL), respectively retaining the same condition. Then the mixture was adjusted to a pH of 9.0 with 6(M) NaOH solution, and stirred for 30 min, yielding a stable light yellow homogeneous emulsion. The resulting mixture was transferred into a 100 mL Teflon-lined stainless steel autoclave and heated to 150 °C for 20-22 h under auto generated pressure. The reaction mixture was allowed to cool to room temperature and the precipitate was filtered, washed with distilled water five times, and dried in a vacuum oven at 100 °C for 1 h and then heated on furnace at different calcination temperatures for removing all the oxides of carbon and water vapours. The composites with different amounts of Cr or Fe and Nb doping will be denoted as the following: $M_xNb_xTi_{1-2x}O_{2-x/2}$, when x = 0.01; M = Cr, as CNT1 and M = Fe as FNT1, x = 0.05; M = Cr, as CNT2 and M = Fe as FNT2, x = 0.1; M = Cr, as CNT3 and M = Fe as FNT3, and x = 0.2; M = Cr, as CNT4 and M = Fe as FNT4, respectively. For comparison, same method was used to synthesize Cr-TiO_2, Fe-TiO_2, Nb-TiO_2 and pure TiO_2. Schematic representations of the sol-gel method for the synthesis of metal nano-composites are shown in SI (Flowchart 1).

Characterization of nanocatalysts

Thermogravimetric (TG) and differential thermal analyses (DTA) (model: DT-40, Shimadzu, Japan) of the precursor powders were carried out in static air at a heating rate of 10 °C/min up to 1000 °C using alumina crucible. The crystal structure of the prepared photocatalysts was measured by X-ray diffractometer (XRD) at room temperature, using a Philips PW1710 diffractometer with Cu Kα as target material using 40 kV accelerating voltage, 30 mA emission current and 4°/min scanning speed. The XRD spectrum of Si crystal was used as a standard to calibrate the scanning angles. Absorbance of Rhodamine B and 4-nitro phenol was measured with the help of UV-VIS spectrophotometer PerkinElmer Lambda 35 (Singapore). Specific surface area and mesoporous characters of the photocatalysts, were determined through Brunauer-Emmett-Teller (BET) gas sorption analysis, which was carried out with a BECKMAN COULTIER SA3100 analyzer. The fine structure of the prepared powders was analyzed by Transmission Electron Microscopy (TEM) (TM-300, Philips). The zeta potential of nanopowders was measured by Zetasizer, Nano-ZS, Malvern, UK.

Photocatalytic experiments

The photocatalytic experiments were carried out by using a 400 W ultrahigh-pressure Hg lamp (PHILIPS-HPL-N, G/74/2, MBF-400) with a maximum emission at about 364 nm as the light source. In all experiments, the reaction temperature was kept at 28 ± 0.5 °C. The photocatalytic activities of the metal oxides $M_xNb_xTi_{1-2x}O_{2-x/2}$ (M = Cr, Fe; x = 0.01-0.2) were conducted as follows:

Reaction suspensions were prepared by adding each photocatalyst nanopowder (0.1 g) into 50 ml of aqueous solution of RhB (0.005 g, 0.1 $mmolL^{-1}$) and p-NP (0.0139 g, 0.1 $mmolL^{-1}$) in a 100 ml quartz beaker in dark condition for about 1 h to reach adsorption equilibrium before photocatalysis. Before introducing $NaBH_4$ solution into the mixture, the reaction container was kept in dark for about 1 h to reach adsorption equilibrium. In aqueous medium, p-NP dissolved slowly forming a light yellow solution. Upon addition of $NaBH_4$ (0.502 mol dm^{-3}), dissolution was quick with the development of a deep yellow colour. The photocatalytic reactions were carried out in a simple cubic system, where the beaker containing the sample was irradiated with UV light (λ > 280 nm) under constant magnetic stirring for varying durations of time. A small aliquot (1 ml) of reactant liquid was picked out at regular intervals of time for analysis. The slurry was then centrifuged at 1500 rpm for 15 min, filtered through a 0.2 μm-millipore filter to remove the suspended particles.

The recovered photocatalysts were re-used for the same experiments after proper washing with distilled water and calcining at 300 °C to check the efficiency for further applications.

Results and discussion

Thermal study and XRD analysis of the compositions

Thermal analyses of the CNT and FNT precursor powder shows that these decompose exothermally with a sharp peak at 348.8 °C and 208.8 °C (shown in **Fig. 1a** and **1b**) respectively. This exothermic peak can be assigned as major decomposition of the metal-TEA complexes. The rate of mass change was observed in the temperature range 100-400 °C. As a result of thermal effect various gases such as CO_2, CO, NO_2, N_2 and H_2O vapor, etc. was evolved which were manifested by a single-step weight loss in the TG curves shown in **Fig. 1a** and **1b**. Above 400 °C there was no significant thermal effect as evident from the DTA curves, and the corresponding TG curves showed no weight loss implying complete volatilization of carbon compounds. The XRD patterns of synthesized nano-composites (CNT1/FNT1, CNT2/FNT2, CNT3/FNT3 and CNT4/FNT4 (Cu-Kα radiation, λ = 1.5408 Å) (**Fig. 1c**) exhibit diffraction peaks at 2θ of 25.2°, 27.2°, 35.9°, 37.8°, 41.2°, 47.8°, 54.2°, 55.2° and 62.4°, which can be readily indexed to the mixture of anatase and rutile phases of TiO_2 [**26, 27**]. The peaks position of 25.2°, 37.8°, 47.8°, 54.2°, 55.2°, 62.4° for anatase (JCPDS card No. 21-1272) and 27.2°, 35.9°, 41.2°, 54.2° for rutile (Card No. 21-1276) phases of TiO_2. Although Cr and Fe are present in the different compositions separately but their XRD (i.e. CNT1/FNT1) looks alike no different phases arises on XRD in spite of the fact that metal ions are still present. The XRD pattern of pure TiO_2 shows the presence of only anatase phase. The samples NT and CT/FT have XRD patterns which matched exactly with anatase crystal reflections in TiO_2.

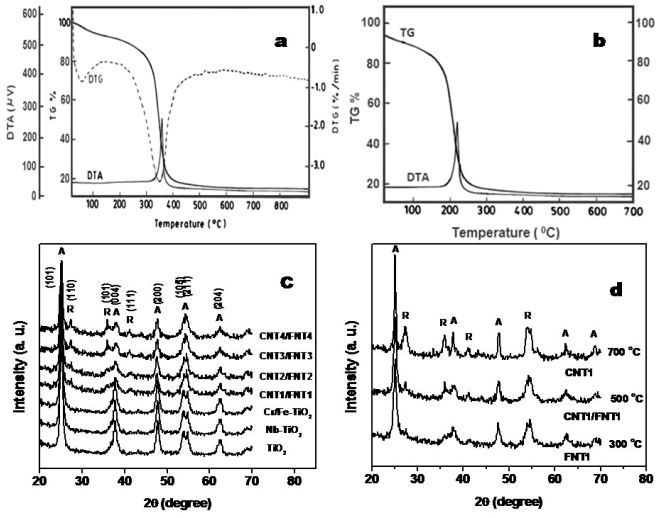

Fig. 1. DTA-TG and DTG of (a) CNT2, (b) FNT2 precursor, (c) XRD patterns of $M_xNb_xTi_{1-2x}O_{2-x/2}$ (where; x = 0.01 (CNT1/FNT1), 0.05 (CNT2/FNT2) 0.1 (CNT3/FNT3) & 0.2 (CNT4/FNT4)), Cr/Fe-TiO_2 (FT), Nb-TiO_2 and pure TiO_2 photocatalyst at 300 °C or above and (d) XRD of FNT1 and CNT1 at different temperatures.

Fig. 1d shows the XRD patterns of CNT1/FNT1 annealed at different temperatures. It indicates that at low temperature (300 °C), FNT1 has a pure anatase TiO_2 crystal structure, and there is no appearance of rutile phase. On increasing the calcination temperatures from 300-700 °C, the anatase phase of FNT1/CNT1 remain same and peak intensity of rutile phase is increased (**Fig. 1d**) and finally gives rise to a mixture of anatase and rutile phases along with grain growth. From thermal analysis observation the exothermic peak point temperature is also accord with the phase formation temperature of XRD. The crystalline size estimated using the Scherrer equation from the full width at half maximum (FWHM) of the (101) peak (2θ = 25.2°) is ~13.7 nm, which is in agreement with the HRTEM observation. All the composites data of crystallite sizes obtained from the diffractograms are presented in **Table 1**.

Table 1. Resultant properties of CNT1, FNT1, CNT2, FNT2, CNT3, FNT3, CNT4, FNT4, NT, CT, FT and P25 TiO_2 nano-composites.

Sample $M_xNb_xTi_{1-2x}O_{2-x/2}$	Acronym	Eg (eV)	S_{BET} (m^2/g)	Crystallites size (nm)	Degradation Rate Const. of Rhodamine B k ($\times10^{-3}min^{-1}$)	Reduction Rate Const.of 4-NP k ($\times10^{-3}min^{-1}$)	Time required for degradation (min) RhB	p-NP
x = 0.01	CNT1/ FNT1	1.85/2.06	162/145	13.70/13.55	35.1/22.8	435.2/589.07	180	10
x = 0.05	CNT2/FNT2	-	125/115.3	13.98/13.83	25.7/10.8	115.2/126.90	210	18
x = 0.1	CNT3/ FNT3	-	59.1/49.1	14.08/13.92	13.0/6.8	25.5/ 55.31	330	35
x = 0.2	CNT4/FNT4	-	45.7/45.7	14.17/14.02	7.6/ -	10.3/43.5	720	48
Nb-TiO_2	NT	2.1	52.7/52.6	12.14	17.5	39.35	270	65
Cr-TiO_2	CT	-	32.33	12.39	7.0	25.12	-	65
Fe-TiO_2	FT	2.3(R20)	32.3	12.41	10.3	37.86	-	68
P25 TiO_2	-	3.2(R20)	49.0	12.42	9.4	32.62	540	80
Absence of catalyst					0.005	23.94	-	82

Eg: Energy Band gap; Const.: Constant; R20: Reference 20; Reaction rate constants were measured after 180 minutes decolorization of RhB and 10 minutes reduction of p-nitrophenol to p-aminophenol in presence of UV light, BET surface area measured by liquid nitrogen adsorption-desorption isotherm at room temperature. Time required in different conditions for reduction of yellow colour of p-nitro phenol to colourless p-amino phenol

TEM and specific surface area analysis

TEM and HR-TEM interpreted the mesoporous structure and crystallization of the CNT1 and FNT1 particles. **Fig. 2(a)** and **(c)** shows a typical TEM image of CNT1 and FNT1 and clearly indicates each particle's shape is a unique. **Fig. 2(b)** and **(d)** represents HRTEM of CNT1 and FNT1 particles and the inset figure indicates SAED pattern of the same sphere and the order of mesoporous structure can be observed in the same HR-TEM images. It also reveals the coexistence of a porous mesostructure and high symmetric order of crystallinity in the CNT1 and FNT1 nano-composites. The particle and mesopore sizes of CNT1 and FNT1 are in the range of 12±1, 10±2 nm and 4.9, 4–5 nm respectively. The surface area and porosity of the CNT1 and FNT1 microspheres are explored using the nitrogen adsorption and desorption isotherm (shown in Supplementary information of **Fig. 1**). It can be seen from this figure that in both cases there is one hysteresis loop that appears in the isotherm. The isotherm can be classified as type IV nature curve with a type H_2 hysteresis loop, indicating the presence of mesoporous materials [**28**]. The inset in each SI 1 shows the pore size distribution calculated by the Barrett–Joyner–Halenda (BJH) method using the desorption isotherm. The BET surface area and pore volume of the mesoporous FNT1 spheres are 162, 145 $m^2\ g^{-1}$ and 0.159, 0.246 $cm^3\ g^{-1}$, respectively. The BET surface areas (SA) of other composites of $M_xNb_xTi_{1-2x}O_{2-x/2}$ are shown in **Table 1**. However, attempts made to prepare the solid solution using the co-precipitation method were unsuccessful. The surface charges of the CNT1 and FNT1 nano-composites at various pH have been investigated by

measuring the electrokinetics (zeta potential) of the particles. The isoelectric point for CNT1 and FNT1 are at pH 5.8 and its zeta potential values are -24 mV and -21 mV at pH 7 and gave high surface area [**6, 29**]. The positive charge over the lower pH range that may be due to the presence of protonated hydroxyl groups ($Ti–OH_2^+$) at the surface, whereas, at higher pH, the protonated surface sites decrease and the zeta potential becomes more negative.

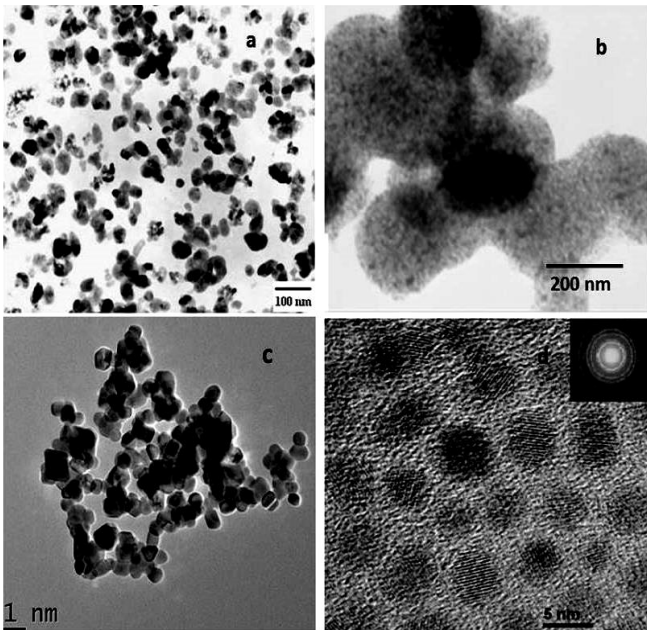

Fig. 2. (a) TEM images of CNT1, (b) Mesoporous structure of CNT1 obtained from HRTEM, (c) TEM of FNT1, (d) Enlarged one FNT1 particle (HRTEM) and SAED pattern of same sphere.

X-ray photoelectron spectroscopy (XPS) analysis

Fig. 3 shows the XPS spectra of FNT1 and CNT1 in a range (binding energy 355-750 eV) covering the photoemission peaks. The photoelectron peak of Nb($3p_{3/2}$) at 365.2 eV in **Fig. 3(a)** indicates +5 oxidation state of Nb. The **Fig. 3(b)** shows two peaks of binding energy of Ti(2p). The peak located at a binding energy of 458.9 eV and 464.5 eV corresponds to the Ti($2p_{3/2}$) and Ti($2p_{1/2}$). The splitting between Ti($2p_{3/2}$), and Ti($2p_{1/2}$) core levels is 5.6 eV indicating a normal state of Ti^{4+} in the anatase FNT1. **Fig. 3(c)** shows the photoelectron peaks at 529.8 eV corresponding to the O (1s). **Fig. 3(d)** shows the XPS spectra covering the Fe (2p) peaks. The Fe (2p) core level is split into $Fe_2p_{3/2}$ and $Fe_2p_{1/2}$ due to spin orbit coupling and appears at their normal positions at 710.8 and 724.7 eV respectively. The XPS spectra do not show any elemental Fe peak. A hump at ~719 eV is characteristic of the presence of Fe^{3+}. **Fig. 3(e)** displays the photoelectron peaks at 577.1 eV and 586.8 eV which correspond to the binding energy of Cr($2p_{3/2}$) and Cr($2p_{1/2}$) of Cr^{3+} being consistent with the values reported by Jaimy *et al.* [**30**]. The splitting between Cr($2p_{3/2}$) and Cr($2p_{1/2}$) core levels is 3.5 eV indicating a normal state of Cr^{3+} in the CNT1. Other binding energy spectrum of CNT1 remains the same. The above results reveal that spectrum of $M_xNb_xTi_{1-2x}O_{2-x/2}$ corresponds to Fe_2O_3, Cr_2O_3, Nb_2O_5 and TiO_2 specimens on the surface. It indicates that the metal ions exist as Fe(III), Cr(III), Nb(V) and Ti(IV).

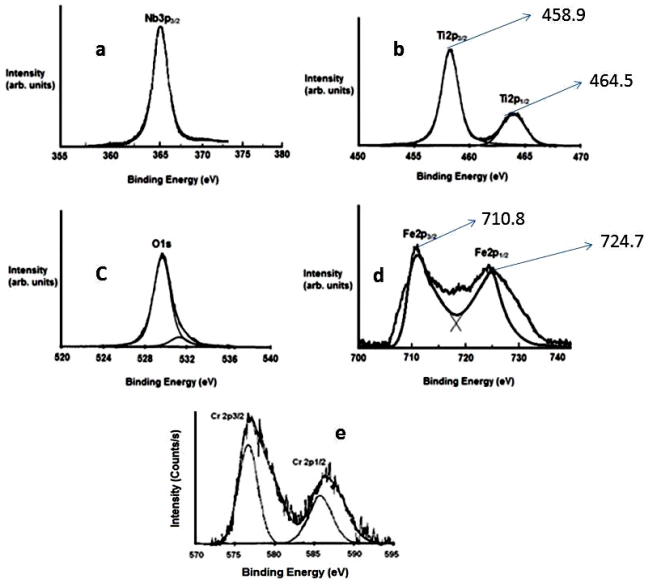

Fig. 3. XPS spectra of FNT1 of ((a) Nb$3p_{3/2}$, (b) Ti$2p_{3/2}$ and Ti$2p_{1/2}$, (c) O1s and (d) Fe$2p_{3/2}$ and Fe$2p_{1/2}$) and CNT1 of (e) Cr$2p_{3/2}$ and Cr$2p_{1/2}$.

Photocatalytic study

Batch adsorption, photocatalysis and photolysis studies of $M_xNb_xTi_{1-2x}O_{2-x/2}$ (M = Cr, Fe)

Adsorption studies were carried out using a standard stock solution of RhB (5 mgL^{-1}) and p-NP (15 mgL^{-1}) prepared by dissolving appropriate amount of RhB and p-NP in deionized water. Compared batch adsorption studies were executed in the 100 ml Erlenmeyer flasks by equilibrating 100 mg of $M_xNb_xTi_{1-}2xO_{2-x/2}$ (Cr, Fe) with 50 ml of working solutions containing different initial RhB and 4-NP concentrations (0, 10, 30, 50, 100, 200, 300 mgL^{-1}) shown in **Fig. 4a** and **4b**, respectively.

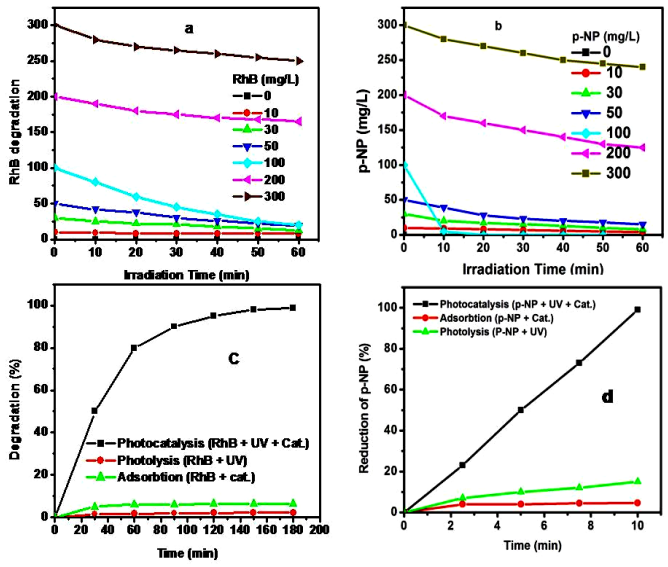

Fig. 4. Batch adsorption studies and comparison of photocatalysis, photolysis and adsorption in different initial RhB and p-NP concentrations (0, 10, 30, 50, 100, 200, 300 mgL^{-1}) and catalysts are shown in Fig a, b and c, d, respectively. Fig. C RhB (100 mg/l, Time: 180 min) and in Fig. (d) 4-NP (100 mg/l, Time: 10 min).

For these experiments, the flasks were capped and shaken at room temperature at 125 rpm for 20 h in a mechanical shaker in the dark condition to attain the adsorption equilibrium. Then, the supernatant was centrifuged, clear water was decanted off and the concentration of RhB and 4-NP in the supernatant was determined via UV-Vis spectrophotometer. The equilibrium adsorption capacity of synthesized nano-composites was determined from the difference in initial and final concentrations of the working solutions. All the adsorption experiments were performed in triplicate for checking reproducibility. Photo degradation and photo reduction efficiency of RhB and p-NP or 4-NP was observed in different conditions i.e. photocatalysis, photolysis and adsorption (shown in **Fig. 4(c)** and Fig. **4(d)**), respectively. In both the cases the conditions of photocatalysis (RhB/p-NP + UV + Catalyst) is the better option for measurement the photocatalytic activity.

Photocatalytic observation of $M_xNb_xTi_{1-2x}O_{2-x/2}$ (M=Cr, Fe)

Fig. 5(a) represents the degradation of RhB in presence of different catalysts under UV light irradiation. It shows that CNT1 is best photoactive (35.1×10^{-3} min^{-1}) and it takes only 180 min for complete degradation of RhB compared to all other synthesized compositions. The changes in concentration of RhB as a function of UV-light exposure time in the presence of the CNT1 photocatalysts in different irradiation time interval are shown in **Fig. 5(b)**. The degradation rate constant (k) for RhB using CNT1, CNT2, FNT1, CNT3, CNT4, FNT2, NT, CT, and TiO_2 photocatalysts have been presented as a function of the time required after 180 min decolorization of dye solution shown in **Table 1**. Increase of the different dopant (Cr and Nb) concentrations in TiO_2 solid solution decreased the rate of photodegradation due to the decrease of specific surface area for the different doped catalysts. **Fig. 5(c)** shows the reduction rate constants of p-NP and synthesized catalysts under UV light. Among all the synthesized catalysts, FNT1 shows the good photo reduction activity of 4-NP and within 10min it reduces p-NP to p-aminophenol (p-Amp) and colour change appears to be yellow to colourless. But in absence of UV light it takes about 20 min for reduction. The other compositions of CNT1, CNT2, FNT2, FNT3, FNT4, CNT4, NT, FT, CT and prepared TiO_2 takes much more time for formation of 4-Amp (**Table 1**). In absence of catalysts and other conditions remaining the same it takes 82 min for complete reduction. The catalytic activity of TiO_2, and the formation of 4-AmP were not observed in presence of UV light. Therefore, FNT1 catalysts give much faster reaction kinetics (5.89×10^{-5} min^{-1}) than that of other compositions of $M_xNb_xTi_{1-2x}O_{2-x/2}$ due to high porousness of the materials and small particle sizes. Reduction rate constant of FNT1 in presence of 4-NP and UV light at small duration time interval was shown in **Fig. 5(d)**. The change in the concentration of 4-NP and FNT1 at different irradiation time interval in presence of UV light is shown in **Fig. 5(e)**. FNT1 catalyst led to a significant decrease of the absorption peak at 415 nm and increase of absorbance peak at 285 nm in UV-vis spectra corresponding to 4-NP. During the reduction, the yellow color faded with the simultaneous formation of a slight shifted peak position and a new peak grows at 294 nm assigned to 4-AmP in UV-vis spectra [**32, 33**]. The complete disappearance of the UV-vis absorption peak at 415 nm of 4-NP occurred at 10 min which indicates the complete reduction of 4-NP to 4-AmP. However, the reduction of 4-NP was not accomplished well even under the condition which uses large excess of $NaBH_4$ in absence of the catalyst.

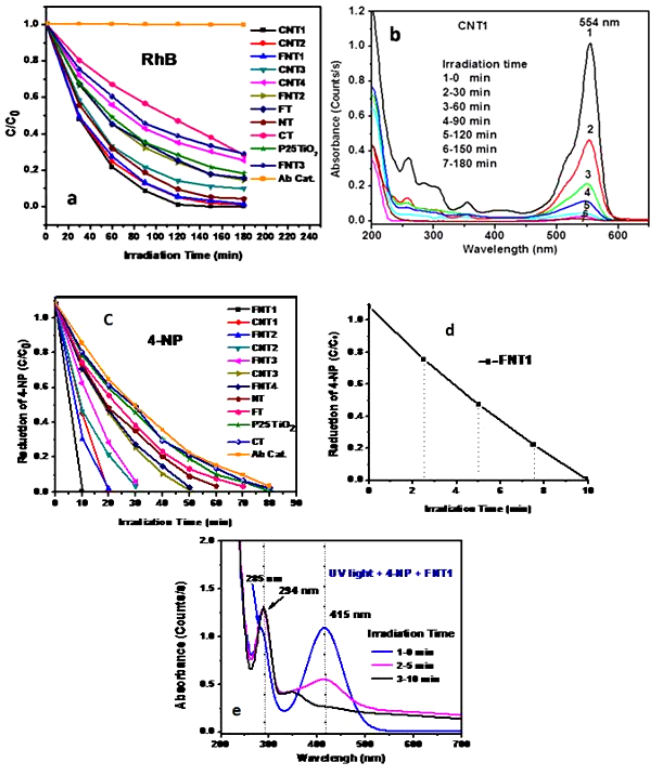

Fig. 5. (a) Degradation of RhB in presence of catalysts and UV light (b) The changes in the concentration of RhB in presence of CNT1 in different irradiation time interval (c) Reduction of 4-NP in presence of catalysts and UV light (d) Reduction rate constant of FNT1 in presence of 4-NP and UV light at small duration time interval (e) The changes in the concentration of 4-NP in presence of FNT1 at different irradiation time interval in presence of UV light.

Band gap measurement and probable mechanistic pathway

UV-Vis absorbance spectra (In set) and corresponding band gap energy of CNT1, FNT1 and NT composition calcined at 300 ^oC are shown in **Fig. 6**. The direct band gap (Eg) of the samples is determined by fitting the absorption data to the direct transition Eq. (1),

$$\alpha h\nu = Ed(h\nu - Eg)^{1/2} \quad (1)$$

where, α is the optical absorption coefficient, hν is the photon energy, Eg is the direct band gap, and Ed is a constant [**31**]. The band gap of prepared sample was measured by plotting $(\alpha h\nu)^2$ as a function of photon energy, and extrapolation the linear portion of the curve to absorption equal to zero as given in top part of **Fig. 6**. The spectra of CNT1, FNT1 and NT indicates the absorption onset at around 670, 602 and 592 nm which is in excellent agreement with band gap of 1.85, 2.06 and 2.1 eV, respectively. The energy band gap of CNT1, FNT1 and NT are much lower compared to TiO_2. It is well established that the conduction band electrons (e^-) and valence band

holes (h^+) are generated when aqueous TiO_2 suspension is irradiated with UV light having energy greater than its band-gap energy (Eg, 3.2 eV). If energy gap of two valence bands are lower, then electron goes from valence band to the conduction band much faster and degrades RhB to produce CO_2 and H_2O (shown in bottom part of **Fig. 6**). On the other hand, $NaBH_4$ itself reduces 4-NP to 4-AmP but in the presence of the catalyst the rate of reduction is much faster (**Fig. 5c**). Fe, Nb and Ti exist as Fe(III), Nb(V) and Ti(IV) oxidation state (supported by XPS) in the FNT composites. Both Fe(III) and Nb(V) are active in UV light, so we cannot precisely say that which ions are responsible for generation of e^-/h^+ pairs. It shows that Fe and Nb are responsible for generation of electron/hole pair through mutual charge transfer from Fe(III) and Nb(V) with Ti(IV) ion in presence of irradiation with light energy (photon) which is equal to or greater than its band-gap energy ΔEg of the photocatalysts. The excited electron from the valence band (Fe^{3+}/Nb^{5+}) is transferred to the empty conduction band (Fe^{2+}/Nb^{4+}). Hence, this Fe^{2+}/Nb^{4+} reduces p-nitrophenol to 4-AmP much faster.

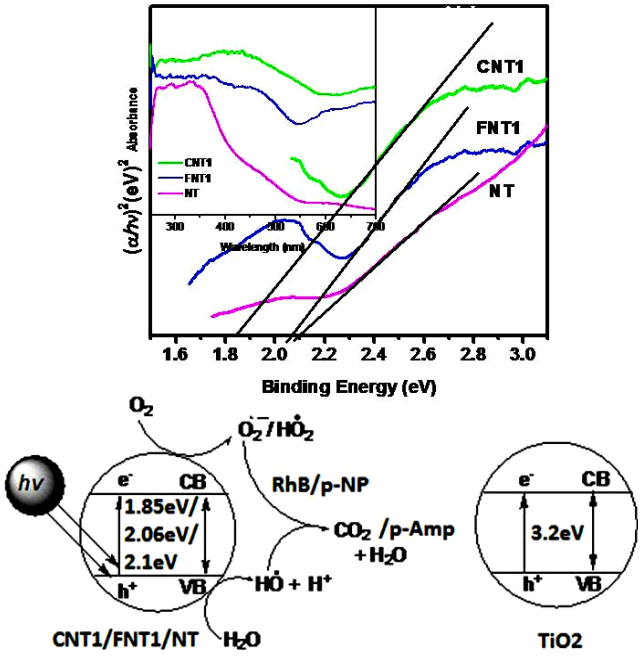

Fig. 6. UV-Vis absorbance spectra (In set) and corresponding band gap energy of CNT1, FNT1 and NT composition calcined at 300 °C shown in the top part and bottom part represent schematic diagram (energy level) of the proposed mechanism of photodegradation and reduction of RhB and p-NP by CNT1/FNT1/NT photocatalysts in presence of UV light.

Conclusion

Nano-composites of Cr(III)/Fe(III) and Nb(V) mixed with TiO_2 lattice were synthesized by conventional sol-gel method and it is found that photo degradation and reduction of RhB and p-NP with CNT1 and FNT1 in presence of UV light can be achieved respectively with high efficiency. The photo degradation and reduction of RhB and p-NP are better in case of CNT1 and FNT1, respectively. The balance between Cr(III)/and Fe(III) and Nb(V) with Ti(IV) states in $Cr_xNb_xTi_{1-2x}O_{2-x/2}$ and $Fe_xNb_xTi_{1-2x}O_{2-x/2}$ is critical to achieve efficient degradation of RhB and p-nitrophenol reduction, respectively. This is probably due to efficient generation of electron and hole under UV light through mutual charge transfer from Cr(III)/Fe(III) and Nb(V) ion in the composites. Furthermore CNT1 and FNT1 has continued to be highly active in photocatalytic applications because of its lower band gap energy (1.85 and 2.06 eV) and high surface area (162 and 145 m^2g^{-1}). Therefore, our main objectives to study the photocatalytic effect on different aspects i.e. photodegradation of organic dye (RhB) and photoreduction of p-NP by synthesized nanocomposites are successfully completed.

Acknowledgements

The authors are grateful to the Department of Science and Technology (DST) as "Fast Track Scheme for Young Scientists" (SR/FT/CS-021/2010), New Delhi, India for the financial grant offered in support of this work.

Author contributions

Conceived the plan: Tanmay K Ghorai; Performed the expeirments: S. Sikdar, S. Pathak; Data analysis: S. Sikdar, S. Pathak & T K Ghorai; Wrote the paper: Tanmay K Ghorai, S. Sikdar, S. Pathak (S. Sikdar, S. Pathak, T K Ghorai are the initials of authors). Authors have no competing financial interests.

Reference

1. Palmisano, L.; Sciavello, M.; Sclafani, A.; Martra, G.; Borello, E.; Coluccia, S. *Appl. Catal. B*, **1994**, *3*, 117-132. **DOI:** 10.1016/0926-3373(93)E0031-6
2. Enachi, M.; Lupan, O.; Braniste, T.; Sarua, A.; Chow, L.; Mishra, Y. K.; Gedamu, D.; Adelung, R.; Tiginyanu, I. *Physica status solidi (RRL)* **2015**, *9*, 171-174. **DOI:** 10.1002/pssr.201570615
3. Wang, D.; Duan, Y.; Luo, Q.; Li, X.; An, J.; Bao, L.; Shi, L. *J. Mater. Chem.*, **2012**, *22*, 4847-4854. **DOI:** 10.1039/C2JM14628B
4. Cushing, S. K.; Li, J.; Meng, F.; Senty, T. R.; Suri, S.; Zhi, M.; Li, M.; Bristow, A. D.; Wu, N. *J. Am. Chem. Soc.*, **2012**, *134*, 36, 15033. **DOI:** 10.1021/ja305603t
5. Zuas, O.; Budiman, H.; Hamim, N. *Adv. Mat. Lett.* **2013**, *4*, 9, 662. **DOI:** 10.5185/amlett.2012.12490.
6. Ghorai, T. K.; Dhak, P. Adv. *Mat. Lett*. **2013**, *4*, 2, 121. **DOI:** 10.5185/amlett.2012.7382
7. Lv, T.; Pan, L.; Liu, X.; Sun, Z. Catal. Sci. Technol., **2012,** *2*, 2297. **DOI:** 10.1039/c2cy20023f
8. He, W.; Wu, H.; Wamer, W. G.; Kim, H. K.; Zheng, J.; Jia, H.; Zheng, Z.; Yin, J. *J. ACS Appl. Mater. Interfaces* **2014**, *6*, 15527. **DOI:** org/10.1021/am5043005
9. Mikaela, S.; Anderson, J. *A. Catal. Sci. Technol*., **2013**, *3*, 879. **DOI:** 10.1039/c3cy20851f
10. Zhang, W.; Zou, L.; Lewis, R.; Dionysio, D. *J. Mater. Sci. Chem. Eng.*, **2014**, *2*, 28. **DOI:** org/10.4236/msce.2014.211005
11. Rasalingam, S.; Peng, R.; Koodali, R. T. *J. Nanomater*. **2014**, *42*. **DOI:** org/10.1155/2014/617405
12. Zhou, X.; Lu, J.; Jiang, J.; Li, X.; Lu, M.; Yuan, G.; Wang, Z.; Zheng, M.; Seo, H. *J. Nanoscale Res. Lett.* **2014**, *9*, 34. **DOI:** 10.1186/1556-276X-9-34.
13. Ismail, A. A.; Bahnemann, D. W. *J. Mater. Chem*. **2011**, *21*, 11686. **DOI:** 10.1039/C1JM10407A
14. Kohn, P.; Pathak, S.; Stefik, M.; Ducati, C.; Wiesner, U.; Steiner, U.; Guldin, S. *Nanoscale*, **2013**, *5*, 10518. **DOI:** 10.1039/C3NR03009A
15. Wang, B.; Guo, L.; He, M.; He, T. *Phys. Chem. Chem. Phys*. **2013**, *15*, 9891. **DOI:** 10.1039/C3CP50862E
16. Mathew, A.; Gowravaram, M. R.; Nookala, M. *Adv. Mat. Lett*. **2013**, *4*, 10, 737. **DOI:** 10.5185/amlett.2013.2423
17. Yan, J.; Wu, G.; Guan, N.; Li, L. *Appl. Catal.B: Environ*. **2014**, 152-153, 280-288. **DOI:** 10.1016/j.apcatb.2014.01.049
18. Kuncewicz, J.; Zabeka, P.; Stochel, G.; Stasicka, Z.; Macyk, W. *Catal. Today* **2011**, 161, 78.

DOI: 10.1016/j.cattod.2010.10.075
19. Chakravadhanula, V. S. K.; Mishra, Y. K.; Kotnur, V. G.; Avasthi, D. K.; Strunskus, T.; Zaporotchenko, V.; Fink, D.; Kienle, L.; Faupel, F. Beilstein J. *Nanotechnol*. **2014**, *5*, 1419.
DOI: 10.3762/bjnano.5.154
20. Ghorai, T. K.; Biswas, S. K.; Pramanik, P. *Appl. Surf. Sci*. **2008**, *254*, 7498.
DOI: 10.1016/j.apsusc.2008.06.042
21. Virkutyte, J.; Varma, R. S. *RSC Adv*. **2012**, *2*, 1533.
DOI: 10.1039/C1RA00990G
22. Gaba, R.; Bhandari, M.; Kakkar, R. *Adv. Mat. Lett*. **2013**, *4*, 10, 769.
DOI: 10.5185/amlett.2013.2424
23. Kuriakose, S.; Satpati, B.; Mohapatra, S. *Adv. Mater. Lett*. **2015**, *6*, 3, 217.
DOI: 10.5185/amlett.2015.5693
24. Kalyamwar, V. S.; Raghuwanshi, F. C. *Adv. Mat. Lett*. **2013**, *4*, 12, 895.
DOI: 10.5185/amlett.2013.4456
25. Ghorai, T. K.; Dhak, D.; Biswas, S. K.; Dalai, S.; Pramanik, P. J. *Mol. Catal. A: Gen*. **2007**, *273*, 224.
DOI: 10.1016/j.molcata.2007.03.075
26. Addamo, M.; Bellardita, M.; Paola, A.D.; Palmisano, L. *Chem. Commun*. **2006**, 4943.
DOI: 10.1039/B612172A
27. Zachariah, A.; Baiju, K.V; Shukla, S.S.; Deepa, K.S.; James, J.; Warrier, K.G.K. *J. Phys. Chem. C*, **2008**, *112*, 30, 11345.
DOI: 10.1021/jp712174y
28. Sing, K.S.W. *Pure Appl. Chem*. **1982**, *54*, 2201.
DOI: 10.1351/pac198254112201
29. Ghorai, T. K. *J Mater. Res. Technol*. **2014**, *4*, 2, 133.
DOI: 10.1016/j.jmrt.2014.11.005
30. Jaimy, K.B.; Ghosh, S.; Sankar, S.; Warrier, K. G. K. *Mater. Res. Bull*. **2011**, *46*, 914.
DOI: 10.1016/j.materresbull.2011.02.030
31. Ziegler, E.; Heinrich, A.; Oppermann, H.; Stover, G. *Phys. Status Solidi A*, **1981**, *66*, 635.
DOI: 10.1002/pssa.2210660228
32. Mitchel, S. C. *Aminophenols, 4th Ed*, **2000**, *2*, 580.
33. Zhang, H.; Yang, X. *Poly. Chem*. **2010**, *1*, 670.
DOI: 10.1039/B9PY00372J

Supporting Information

Experimental Setups/Schematics

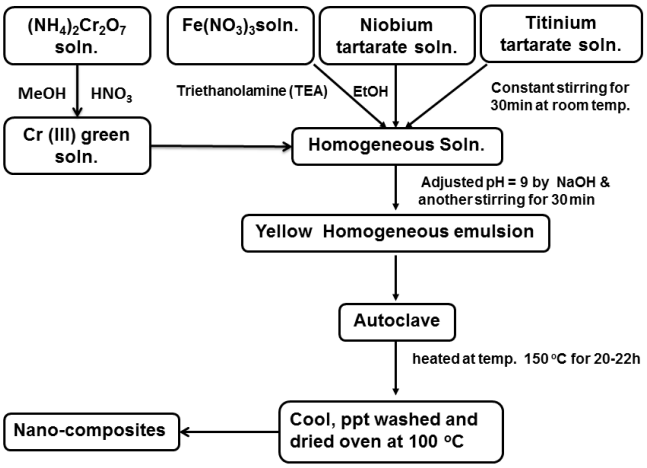

Scheme 1. Flowchart representation of the sol-gel method for the synthesis of MxNbxTi1-2xO2-x/2 (M = Cr, Fe; x= 0.01, 0.05, 0.1, 0.2 mol%) nano-composites.

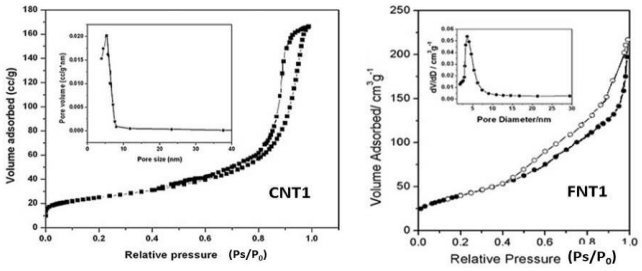

Fig. 1. N_2 adsorption-desorption isotherm and a pore size distribution curve (inset) of CNT1 and FNT1